Journal of Alloys and Compounds 505 (2010) 379–384

Contents lists available at ScienceDirect

Journal of Alloys and Compounds

journal homepage: www.elsevier.com/locate/jallcom

Studies of oxidized carbon nanotubes in temperature range RT–630 °C by the infrared and electron spectroscopies

L. Stobinski[a,b], B. Lesiak[a,*], J. Zemek[c], P. Jiricek[c], S. Biniak[d], G. Trykowski[d]

[a] Institute of Physical Chemistry, Polish Academy of Sciences, Kasprzaka 44/52, 01-224 Warsaw, Poland
[b] Faculty of Materials Science and Engineering, Warsaw University of Technology, Wołoska 141, 02-507 Warsaw, Poland
[c] Institute of Physics, Academy of Sciences of the Czech Republic, Cukrovarnicka 10, 162 53 Prague 6, Czech Republic
[d] Department of Chemistry, Nicolaus Copernicus University in Toruń, Gagarina 7, 87-100 Toruń, Poland

ARTICLE INFO

Article history:
Received 13 January 2010
Received in revised form 19 May 2010
Accepted 28 May 2010
Available online 18 June 2010

Keywords:
Multiwall carbon nanotubes
Functionalization
Temperature modification
Infrared spectroscopy
Electron spectroscopy

ABSTRACT

The oxidized multiwall carbon nanotubes, their temperature modification in the range from RT to 630 °C are studied. The oxidation proceeds in aqueous solution of the concentrated HNO_3. The oxidized multiwall carbon nanotubes are investigated using the infrared and electron spectroscopy methods.

The oxidation creates mainly carboxyl, hydroxyl and carbonyl groups attached to multiwall carbon nanotubes, which can be detected by the infrared spectroscopy and at the surface by the electron spectroscopy methods. Thermal modification under ultra-high vacuum conditions leads to decreasing content of water, oxygen and carbon groups proceeding with different rates, increasing content of C sp^2 bonds (*e.g.* carbon nanotubes reconstruction), surface atoms ordering and changes of surface atomic density.

1. Introduction

The carbon nanotubes (CNTs) [1] are the most interesting carbon materials opening promising technological applications in nanotechnology, biochemistry, biomedicine, catalysis, electronics, optoelectronics, electrochemistry or space industry [2–4]. The CNTs are the carbon allotropic form built from the rolled graphene (the single atomic graphite layer) sheets. The CNTs consist mainly of C sp^2 hybridizations, however defects, other atoms and chemical groups introduce the C sp^3 bonds. The CNTs exist in a wide variety of forms, *i.e.* the single walled carbon nanotubes (SWCNTs), the multiwall carbon nanotubes (MWCNTs) of different structures and modified with different chemical groups and metallic/nonmetallic nanoparticles [5]. The CNTs are characterized by the unique physical and chemical properties. However the changes in these properties and in the mechanism of physical and chemical processes may be introduced due to surface and bulk modifications, especially with metallic nanoparticles.

The recent applications of carbon nanomaterials, such as CNTs, have been focused on the hydrogen storage, hydrogen production, solar and fuel cells and new composite materials. The fuel cell technology has become a project of high concern due to its crucial significance for practical utilization of hydrogen (or other biofuels) energy replacing carbon, oil and gas. The application of CNTs in fuel cell and hydrogen storage systems has been described elsewhere [5–7]. The fuel cells operate using hydrogen, methanol or formic acid, oxygen as reactants and produce electrical current, water and in some cases carbon dioxide, being the cleanest and the most efficient energy technology. The CNTs based catalysts were shown to perform more effectively than the carbon black supported [6–9]. Recently, the Pd-Au on MWCNTs has been shown to be an efficient catalyst of formic acid electrooxidation [6,7]. The CNTs and carbon nanofibres (CNFs), exhibit a number of features typical for a promising component of an anode catalyst layer, *i.e.* the high electrical and thermal conductivity (especially MWCNTs), the large specific surface area, leading to high concentration of metal surface sites in the catalytic layer and access for the reactants to catalysts metal nanoparticles deposited on the surface. It was demonstrated that the replacement of carbon black by CNTs decreases the agglomeration rate of metal catalyst nanoparticles, which supports efficiency of electrooxidation

* Corresponding author. Tel.: +48 22 343 3432; fax: +48 22 632 5276.
E-mail address: blo@ichf.edu.pl (B. Lesiak).

0925-8388/$ – see front matter © 2010 Elsevier B.V. All rights reserved.
doi:10.1016/j.jallcom.2010.05.185

Table 1
The assignment of absorption bands from the FTIR spectra.

Frequency range (cm^{-1})	Assignment	Possible structural groups
3600–3100	O–H	H_2O, surface OH groups (hydroxyl, carboxyl)
3010–3040	C–H stretching vibration	C sp^2 – alkene and aromatic systems
2860–2950	C–H stretching (symmetric and asymmetric)	C sp^3 – alkane (methyl, methylene) systems
1800–1650	C=O stretching vibration	Carboxyl, ester, lactonic, acid anhydride groups, unsaturated ketones, quinines, carboxylic groups in aromatic ring
1650–1500	)C=C(stretching vibration	Aromatic rings, conjugated alkene systems
1415, 1430	=C–H_2	C sp^2
1430–1450	)C=C(stretching vibration	Polynuclear aromatic systems
1375, 1398, 1450, 1480	–C–H	C sp^3
1350–1000	Combination of C–O stretching vibration and O–H deformation, symmetric and asymmetric =C–O stretching, C–O–C (ring) vibration	Aromatic and unsaturated alcohols, phenols hydroquinine; cyclic, diaryl ethers; oxirane (epoxides) systems; ketals and acetals, aromatic dioxy compounds
1250–1000	=C–H in plane deformation	Aromatic systems (mono-, di-substituted)
600–650	In plane ring vibration	Polynuclear aromatic systems

[10,11]. The characterization of electrodes allows for optimizing the structure/geometry, the operational parameters, the stability, the lifetime and for determining the catalysts optimum composition and structure. The extensive studies on MWCNTs supported with metallic nanoparticles [5–9], the purification and functionalization of the MWCNTs support [12] have already been started.

In the present work the multiwall carbon nanotubes oxidized by a concentrated nitric acid (denoted as ox-MWCNTs) and their derivatives obtained by annealing from RT to 630 °C are investigated using the Fourier transform infrared spectroscopy (FTIR) and electron spectroscopy methods, like X-ray excited Auger electron spectroscopy (XAES), X-ray spectroscopy (XPS), elastic peak electron spectroscopy (EPES) and reflection energy loss spectroscopy (REELS).

2. Experimental

2.1. Samples

The samples of "as-received" MWCNTs (CNT CO., LTD., Korea) were oxidized in boiling 68 wt% concentrated HNO_3 under a reflux condenser (about 50 h at 118 °C) and then rinsed with deionised H_2O till stabilization of filtrate pH.

2.2. Infrared spectroscopy

The obtained oxidized material (ox-MWCNTs) was divided into several samples and each portion was heated at temperatures 200 °C, 300 °C, 400 °C, 500 °C and 600 °C under pressure of 10^{-3} Torr. The FTIR spectra of obtained samples were measured by the infrared Fourier transform spectrometer (Spectrum 2000, Perkin Elmer, Germany) in the range of 400–4000 cm^{-1}. The samples were mixed with KBr, heated at 100 °C under vacuum ($p = 10^{-3}$ Torr) to remove traces of H_2O and finally pressed in a hydraulic press.

2.3. Electron spectroscopy methods

Before the measurements ox-MWCNTs were annealed carefully in UHV from RT to 630 °C. The pressure of desorbing gases did not exceed the value of 10^{-6} Torr. The spectra were recorded at RT in the UHV chamber of ADES-400 electron spectrometer (VG Scientific, UK) equipped with angular-resolved electron analyzer, an electron gun (Varian, model 981-2455) and the X-ray excitation source.

The XPS/XAES spectra were measured using the MgK_α radiation of $h\nu = 1253.6$ eV. The XPS C 1s, O 1s spectra were recorded using the pass energy, $E_p = 20$ eV, whereas the XAES C KLL spectra using the pass energy, $E_p = 100$ eV, with the X-ray incidence angle of 70° and the photoelectrons and Auger electrons emission angle of $\alpha_{out} = 0°$, with respect to the surface normal. For the XPS/XAES spectra, the binding energy (*BE*) reference is the Fermi energy and the kinetic energy (*KE*) reference is vacuum level.

The EPES/EELS spectra were recorded using a defocused primary electron beam of $KE = 1500$ eV and 2000 eV, the beam current of 1×10^{-6} A, a spot of $2r = 3$ mm, $E_p = 20$ eV, within a conical analyzer acceptance angle of ±4.1°, the electron beam incidence angle of $\alpha_{in} = 0°$, the emission angle of $\alpha_{out} = 35°$, with respect to the surface normal.

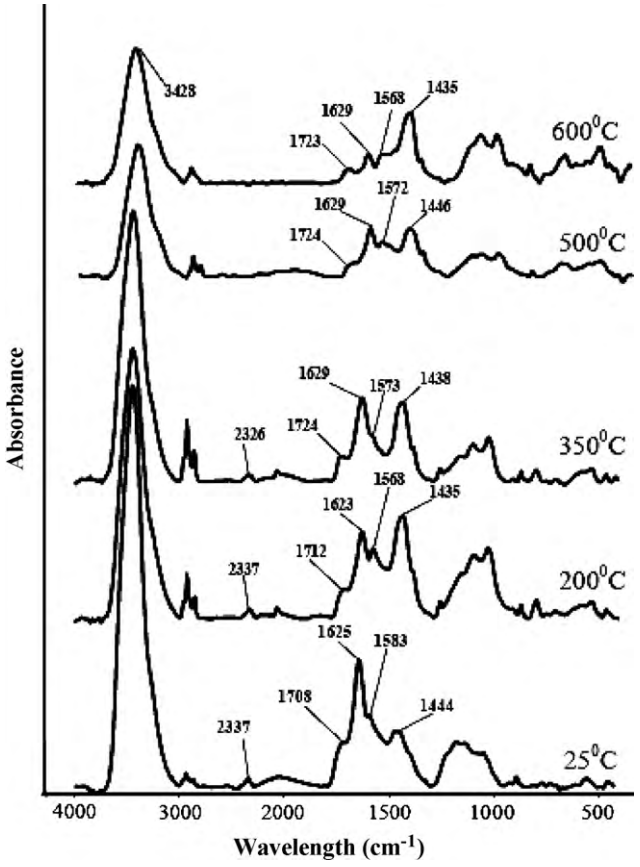

Fig. 1. The FTIR spectra of ox-MWCNTs under annealing.

3. Results

3.1. The infrared spectroscopy

The characteristic absorption bands found in the FTIR spectra recorded for oxidized, not annealed carbon nanotubes, samples annealed gradually up to 600 °C are shown in Fig. 1. The infrared assignments of main bands observed for groups containing C, O and H atoms are compared to those observed for surface groups in carbon nanofibres and amorphous carbon [13]. The compilation and description of absorption bands present in the FTIR spectra of ox-MWCNTs are listed in Table 1.

Table 2
Comparison of C and O atomic content, the positions of C 1s and O 1s peaks, the C sp^2 content resulting from C 1s spectra fitting and evaluation of the width of C KLL spectra.

ox-MWCNTs conditions	XPS (at%)		Peak positions (eV)		XPS C sp^2 (%)	
	C	O	C 1s	O 1s	C KLL	C 1s
RT	87.6	12.4	284.4	532.8	63	82
150 °C-3 h	90.2	9.8	284.5	532.9	74	79
350 °C-1 h	91.8	8.2	284.4	533.0	89	81
465 °C-4.5 h	86.5	13.5	284.4	531.6	96	83
533 °C-2 h	90.1	9.9	284.5	531.5	96	79
590 °C-4 h	91.0	9.0	284.5	531.8	96	83
630 °C-3 h	92.7	7.3	284.4	531.9	96	83

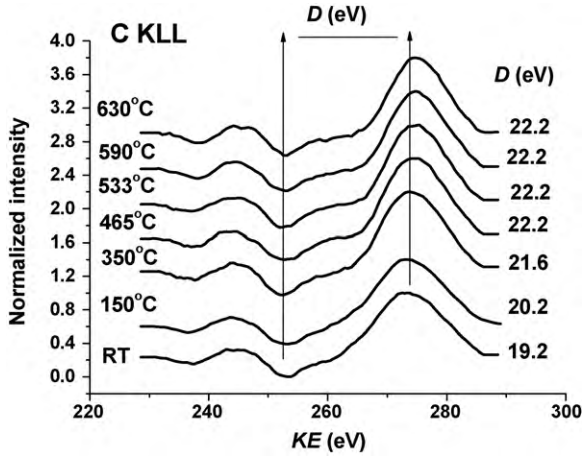

Fig. 2. The first derivative C KLL spectra recorded from ox-MWCNTs after annealing at different temperatures indicating the width of the spectrum (parameter *D*).

3.2. XPS quantitative analysis

The surface atomic content was quantified from XPS C 1s and O 1s transitions by the relative sensitivity factor method [14]. The atomic content of C and O in ox-MWCNTs samples from RT to 630 °C is listed in Table 2.

3.3. Evaluation of C sp^2/sp^3 ratio

The Auger electron transition consisting of the C KV (2pπ)V(2pπ) and C KV (2pσ)V(2pπ) transitions results in a large value of full width at half-maximum (FWHM). The main contribution at *KE* of 272 eV is due to pπ electrons characteristic for C sp^2 hybridizations. The experimental data indicates the changes in the line shape and the FWHM width of the C KLL transition for diamond and graphite. The width between the maximum and the minimum of the first derivative C KLL spectra for diamond (C sp^3) and graphite (C sp^2) varying from 13.2 eV to 22.6 eV, respectively, is called a parameter *D* [15–17]. Its linear interpolation with the C sp^2 content allows evaluating the C sp^2/sp^3 hybridizations. The C KLL spectra recorded from ox-MWCNTs, the estimated parameter *D* and the content of C sp^2 bonds are shown in Fig. 2.

3.4. Content of carbon and oxygen groups

The XPS spectra consist of photoelectron transitions from atoms of different chemical configurations, characterized by the *BE* values. The positions of C 1s and O 1s peaks recorded from ox-MWCNTs are listed in Table 2. However, these spectra consist of photoelectron C 1s and O 1s transitions from C and O atoms of different bonding configurations. The evaluation of C and O atomic bonding content is based on the fitting of C 1s and O 1s spectra using a sum of Gaussian–Lorentzian asymmetric functions, where the *BE* values for expected transitions, assuming the aromatic carbon forms, are taken from the literature compiling the experimental and measured *BE* values for carbon materials [18]. The respective values of *BE* are listed in Table 3. For C sp^2 and C sp^3 components of C 1s spectrum the *BE* separation value of 0.9 eV was assumed due to the agreement of experimental and theoretical values for diamond (C sp^3) and graphite (C sp^2) [19]. The results of fitting of C 1s and O 1s spectra from ox-MWCNTs to different functional C and O groups using asymmetric Gaussian–Lorentzian functions are shown in Figs. 3 and 4, respectively.

The content of C and O functional groups, with *BE* values indicated in Table 3, is normalized to the total area under respective spectra, respectively. The content of C 1s and O 1s functional groups in ox-MWCNTs as a function of temperature, fitted to a polynomial, is shown in Fig. 5(a) and (b), respectively.

3.5. EPES REELS spectra

The REELS can be applied for characterizing some physical properties, like dielectric constant, atomic density and other related quantities [20]. From the knowledge of π and π + σ plasmon energy values and intensities, assuming the nearly free electron approximation, it is possible to evaluate the density of valence electrons, the density of carbon material, the C sp^2/sp^3 fraction, *etc.* The EPES and EPES REELS spectra of electrons quasi-elastically backscattered from atoms and their low energy side of electrons undergoing inelastic losses indicate the structural changes under temperature. These changes are indicated by the values of FWHM, the energies of π loss peak and the changes of area ratio of π loss peak to EPES peak recorded from ox-MWCNTs under annealing. The respective values are indicated in Table 4. Comparison of EPES REELS spectra recorded from ox-MWCNTs at RT and 630 °C recorded at

Table 3
The *BE* values for C 1s and O 1s transitions applied in the fitting procedure.

C 1s bond	*BE* (eV)	O 1s bond	*BE* (eV)
sp^2 graphite	284.2	C=O* carbonyl	531.3
sp^3 diamond	285.1	–C(O*)–O–C– ester	532.0
C*–OH hydroxyl, phenol	286.2	–C(O*)–O–C(O*)– acid anhydride	532.6
C*=O carbonyl	286.8	HO–C=O* carboxyl	533.2
–C*(O)–O–C– ester	288.8	C–O*H hydroxyl, phenol–C(O)–O*–C– ester	533.6
HO–C*=O carboxyl	289.0	–C(O)–O*–C(O)– acid anhydride	533.9
–C*(O)–O–C*(O)– acid anhydride	289.1	HO*–C=O carboxyl	534.5
		H_2O water	535.7

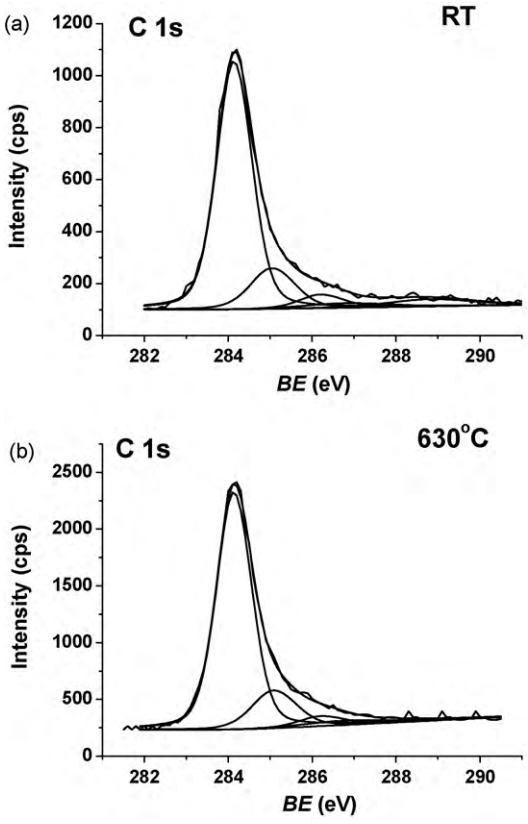

Fig. 3. The C 1s spectra recorded from ox-MWCNTs fitted to carbon functional group components by asymmetric Gaussian–Lorentzian functions. (a) RT. (b) 630 °C.

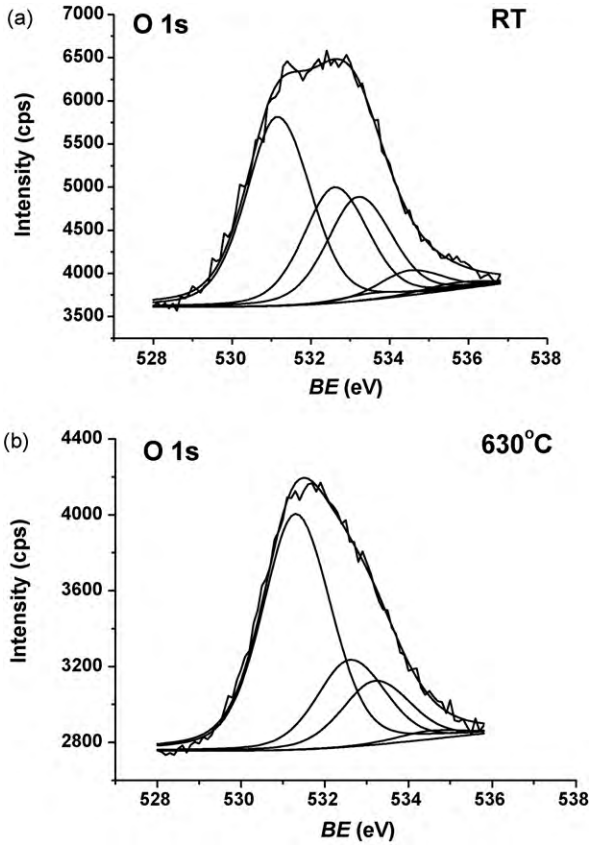

Fig. 4. The O 1s spectra recorded from ox-MWCNTs fitted to oxygen functional group components by asymmetric Gaussian–Lorentzian functions. (a) RT. (b) 630 °C.

different kinetic energies of primary electrons is shown in Fig. 6(a) and (b).

4. Discussion

As shown previously [12] by the elemental analysis, EDS and XPS, the ox-MWCNTs material consisting of C, N, O and H (with N absent at the surface) are in-depth inhomogeneous. The XPS quantitative analysis indicates only the presence of carbon and oxygen at the surface (Table 2). The FTIR analysis at RT provides the evidences for water, hydroxyl and carboxyl groups, carbonyl, ketone, acid anhydride, ester groups, C–H from ≡CH, =CH_2, –CH_3, C sp^3 and C–O–C from ether and acid anhydride groups, present in the bulk (Table 1) [13]. The identified vibration frequencies at 3222 cm^{-1}, at 1711 cm^{-1} and at 1628 cm^{-1} can be ascribed to –OH, –COOH, and C=C or C=O groups, respectively. The C–H stretching in the region from 3010 cm^{-1} to 3040 cm^{-1} are ascribed to sp^2 =C–H mode, whereas in the region from 2860 cm^{-1} to 2950 cm^{-1} to the sp^3 –C–H mode. Otherwise, the sp^2 –C–H stretching modes appear at 1415 cm^{-1} and 1430 cm^{-1}, and sp^3 –C–H stretching modes at 1375 cm^{-1}, 1398 cm^{-1}, 1450 cm^{-1}, 1480 cm^{-1} (Table 1) [13].

Under annealing of ox-MWCNTs the FTIR spectra demonstrate: (i) the relative decrease of band of OH moieties (3600–3100 cm^{-1} and 1627 cm^{-1}) as a result of water molecules desorption, dehydratation of surface functionalities, and finally – destruction of hydrogen-containing groups, (ii) the relative decrease of C=O moieties (existing in various surroundings) as a result of destruction of surface carboxylic groups (1710 cm^{-1}) and keto-enol like surface systems (1625 cm^{-1}), (iii) the relative increase of bands described to polynuclear aromatic systems (1430 cm^{-1}, 650 cm^{-1}) and (iv) the relative increase of CH (sp^3) bands in first stage of annealing (2900 cm^{-1}) and decrease at higher temperatures. The clear evidence for increasing of the C sp^2 bonds accompanied by decreasing of the C sp^3 bonds is given by intensities at about 1430 cm^{-1} (sp^2) and 1480 cm^{-1} (sp^3), respectively (Table 1). The ratio of C sp^2/C sp^3 intensities increases few times from RT to 600 °C (Table 1) [13]. Additionally, the increase of intensity at 2323 cm^{-1}, assigned to COO^- modes, can indicate removing of carbon–oxygen groups and rearrangement and reconstruction of C sp^3 into C sp^2 bonds.

Table 4
Comparison of the FWHM, the π energy loss in the EPES REELS spectra and the ratio of π loss peak to the EPES peak recorded from ox-MWCNTs under annealing.

ox-MWCNTs conditions	EPES 1500 eV			EPES 2000 eV		
	FWHM (eV)	π (eV)	A(π)/A(EPES) (%)	FWHM (eV)	π (eV)	A(π)/A(EPES) (%)
RT	0.78	6.7		0.97	7.3	
150 °C-3 h	1.06			1.18	6.2	4.0
350 °C-1 h	1.13	6.3	1.1	1.24	6.4	1.4
465 °C-4.5 h	0.82	6.4	4.6	0.91	6.3	4.7
533 °C-2 h	0.83	6.5	4.8	0.95	6.3	4.3
590 °C-4 h	0.83	6.5	4.3	0.95	6.3	4.4
630 °C-3 h	0.83	6.5	4.3	0.99	6.4	4.7

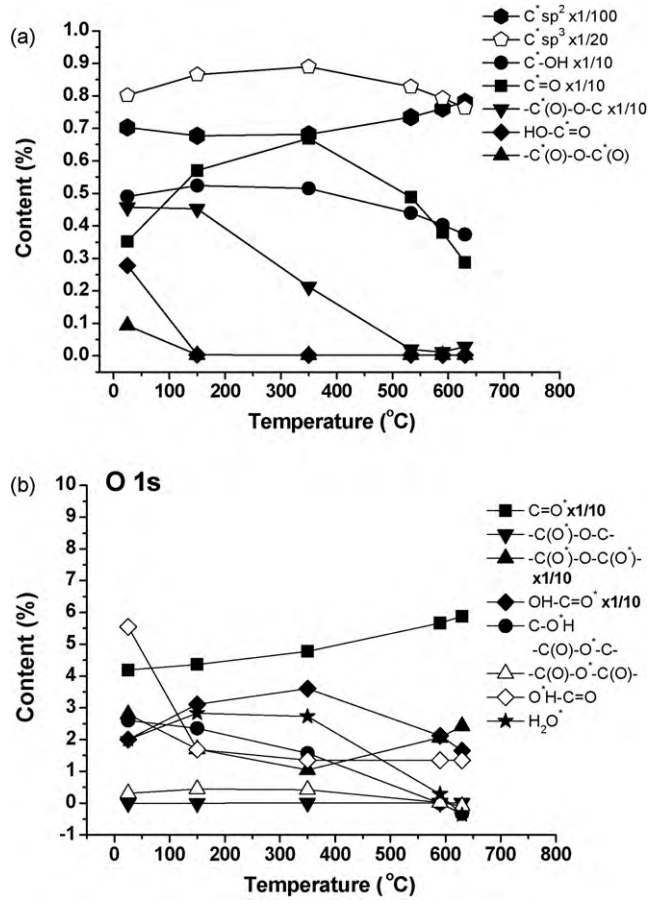

Fig. 5. The content of (a) C chemical groups and (b) O chemical groups under annealing.

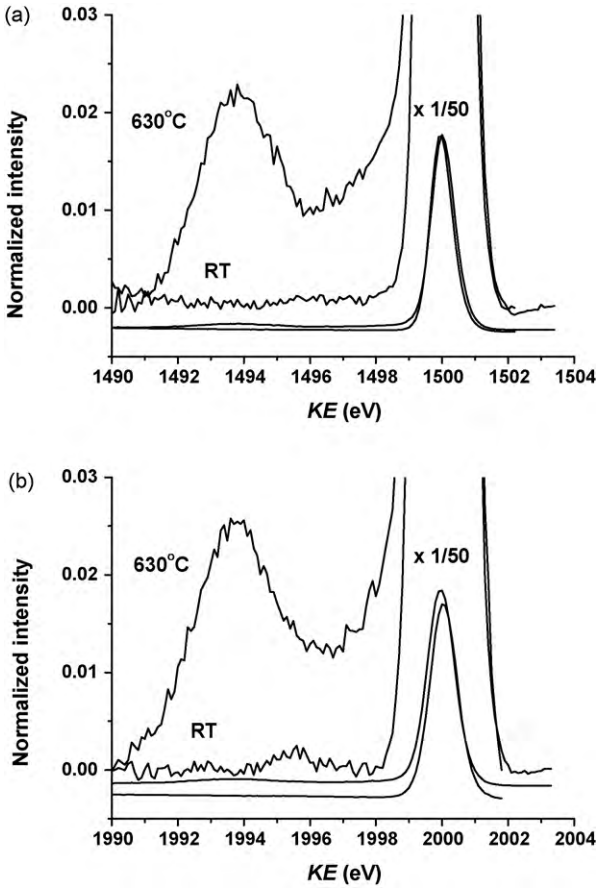

Fig. 6. Comparison of EPES REELS spectra from ox-MWCNTs at RT and 630 °C. (a) *KE* = 1500 eV. (b) *KE* = 2000 eV.

The results of electron spectroscopy methods indicating the surface changes under temperature treatment are consistent with the results of the FTIR spectroscopy. The annealing causes the continuous increase of atomic percent of carbon, accompanied by decrease of oxygen atomic content. The positions of C 1s peaks are nearly constant remaining in agreement with the theoretical and measured values for graphite, *i.e.* 284.4 eV [21], whereas the positions of O 1s peaks shift towards the low *BE* values, indicating decreasing content of carboxyl and hydroxyl groups with remaining groups of oxygen bonded to carbon, *i.e.* carbonyl and carbon-bridged groups (Table 2). Annealing causes an initial increase of C sp^3 functional groups and then their decrease, accompanied by a continuous increase of C sp^2 groups, *i.e.* C bonds reconstruction (Figs. 1 and 5(a)). The C sp^2 hybridization content increases continuously reaching a continuous value of 96% at 630 °C (Table 2, Fig. 2). To the temperature of 350 °C, the increase of FWHM of EPES peaks, accompanied by the π peak shift is observed (Table 4), indicating the structural changes of ox-MWCNTs surface [20,22]. From 350 °C to 630 °C, the decrease of FWHM to constant value is observed, whereas the π loss peak energy remains constant. However, the ratio of area under the π peak and the EPES spectrum increases (Table 4), indicating changes of surface C sp^2/sp^3 ratio and density [20]. These changes result from desorption and removal of carbon–oxygen functional groups, which under annealing undergo decreases with different rate (Fig. 5). The rate of decrease is the most rapid for acid anhydride, carboxyl, whereas ester, hydroxyl and carbonyl undergo a decrease with a slower rate (Fig. 5). The obtained results are consistent with data by Kundu et al. [23]. As shown there [23], carboxyl and ester decompose in the temperature range of 300–440 °C, whereas acid anhydride at about 430 °C. Decomposition of hydroxyl and carbonyl starts at about 590 °C. As confirmed by the mass spectroscopy, to the temperature above 100 °C the predominant contribution to desorption is given by H_2 and H_2O, whereas from 150 °C to 350 °C, the major contribution to desorption is given by CO_2 and CO. Above 465 °C, the increase of CO and decrease of CO_2 contribution are observed. The acid anhydride decomposes into CO_2 and CO, whereas carboxyl into CO. The obtained results using the XPS spectra fitting (Fig. 5) are consistent with the mass spectroscopy, indicating the most rapid decomposition of acid anhydride and carboxyl, whereas the slower rate of ester, hydroxyl and carbonyl decomposition.

5. Conclusions

The applied oxidation reaction results in creating the carboxyl, hydroxyl, carbonyl, acid anhydride and ester groups attached to MWCNTs, which can be detected by the FTIR and XPS spectroscopes. The thermal treatment of ox-MWCNTs up to 630 °C leads to decreasing content of oxygen (from 12.4 at% to 7.3 at%), removing water, carbon and oxygen groups proceeding with different rates. This is accompanied by increasing content of C sp^2 bonds (up to 96%), *i.e.* MWCNTs reconstruction, increasing of carbon atoms surface ordering and changing the atomic density. Different functional groups are decomposed with a various rate. In the temperature range from 300 °C to 440 °C the most rapid decrease rate is observed for acid anhydride and carboxyl. Then, ester, hydroxyl and carbonyl (at about 590 °C) undergo a decrease with a slower rate (Fig. 5). The changes at the surface are more rapid in the temperature range from RT to 465 °C, whereas in the range from 465 °C to 630 °C they are less significant.

Acknowledgments

This work was supported by the exchange project between Polish Academy of Sciences and Czech Science Foundation, Projects No 202/09/0428, AV0Z10100521, Projects of the Polish Council for Science: NN 507 378 235, the Development Grants for the years 2008–2011 (No 15-0011-04/2008, KB/72/13447/IT1-B/U/08) and the Scientific Net BIONAN.

References

[1] L. Stobiński, D.-C. Tien, C.-Y. Liao, H.-M. Lin, W.-S. Kai, Surf. Coat. Technol. 200 (2006) 3203–3205.
[2] Y.-F. Hsiou, Y.-J. Yang, L. Stobinski, W. Kuo, C.-D. Chen, Appl. Phys. Lett. 84 (2005) 984–986.
[3] M. Bonarowska, K.-N. Lin, M. Legawiec-Jarzyna, L. Stobinski, W. Juszczyk, Z. Kaszkur, Z. Karpinski, H.-M. Lin, Solid State Phenom. 128 (2007) 261–271.
[4] S. Iijima, Nature 354 (1991) 56–58.
[5] C.-K. Poh, S.-H. Lim, H. Pan, J. Lin, J.-Y. Lee, J. Power Sources 176 (2008) 70–75.
[6] C.-H. Chen, W.-J. Liou, H.-M. Lin, S.-H. Wu, A. Borodzinski, L. Stobinski, P. Kedzierzawski, Fuel Cells 10 (2) (2010) 227–233.
[7] C.-H. Chen, W.-J. Liou, H.-M. Lin, S.-H. Wu, A. Mikolajczuk, L. Stobinski, A. Borodzinski, P. Kedzierzawski, K. Kurzydlowski, Phys. Status Solidi (a) 207 (2010) 1160–1165.
[8] W.-Z. Li, C.-H. Liang, J.-S. Qiu, W.-J. Zhou, H.-M. Han, Z.-B. Wie, G.-Q. Sun, Q. Xin, Carbon 40 (2002) 791–794.
[9] W.-Z. Li, C.-H. Liang, W.-J. Zhou, J.-S. Qiu, Z.-H. Zhou, G.-Q. Sun, Q. Xin, J. Phys. Chem. B 107 (2003) 6292–6299.
[10] A. Borodziński, G.C. Bond, Cat. Rev. 48 (2006) 91–144.
[11] A. Borodziński, G.C. Bond, Cat. Rev. 50 (2008) 379–469.
[12] B. Lesiak, J. Zemek, P. Jiricek, L. Stobinski, Phys. Status Solidi (b) 246 (2009) 2645–2649;
L. Stobinski, B. Lesiak, L. Kövér, J. Tóth, S. Biniak, G. Trykowski, J. Judek, J. Alloys Compd 501 (1) (2010) 77–84.
[13] S. Biniak, M. Pakuła, A. Świątkowski, M. Walczyk, in: A.P. Terzyk, P.A. Gauden, P. Kowalczyk (Eds.), Carbon Materials: Theory and Practice, Research Signpost, Trivandrum, Kerala, India, 2008, p. 51 (chapter 5);
J. Robertson, Mater. Sci. Eng. R 37 (2002) 129–281.
[14] J.F. Moulder, W.F. Sticle, P.E. Sobol, K.D. Bomben, Handbook of X-ray Photoelectron Spectroscopy, Perkin-Elmer Co, Eden Prairie, MN, 1992.
[15] Y. Mizokawa, T. Miyasato, S. Nakamura, K.M. Geib, J. Vac. Sci. Technol. A 5 (1987) 2809–2814.
[16] S.T. Jackson, R.G. Nuzzo, Appl. Surf. Sci. 90 (1995) 195–203.
[17] J.C. Lascovich, S. Scaglione, Appl. Surf. Sci. 78 (1994) 17–23.
[18] G. Beamson, D. Briggs, High Resolution XPS of Organic Polymers. The Scienta ESCA 300 Database, J Wiley and Sons, Chichester, 1992.
[19] R. Haerle, E. Riedo, A. Pasquarello, A. Baldereschi, Phys. Rev. B 65 (2001) 045101–45109.
[20] L. Calliari, S. Fanchenko, M. Filippi, Diamond Relat. Mater. 16 (2007) 1316–1320.
[21] F.R. McFeely, S.P. Kowalczyk, L. Ley, R.G. Cavell, R.A. Polak, D.A. Shirley, Phys. Rev. B9 (1974) 5268–5311.
[22] S. Lizzit, L. Petaccia, A. Goldoni, R. Larciprete, Ph. Hofmann, G. Zampieri, Phys. Rev. B76 (2007) 153408–153414.
[23] S. Kundu, Y. Wang, W. Xia, M. Muhler, J. Phys. Chem. C 112 (2008) 16869–16878.